

Thermodynamics of the two-component Fermi gas with unequal masses at unitarity

K. M. Daily¹ and D. Blume¹

¹*Department of Physics and Astronomy, Washington State University, Pullman, Washington 99164-2814, USA*

(Dated: October 26, 2018)

We consider mass-imbalanced two-component Fermi gases for which the unequal-mass atoms interact via a zero-range model potential with a diverging s -wave scattering length a_s , i.e., with $1/a_s = 0$. The high temperature thermodynamics of the harmonically trapped and homogeneous systems are examined using a virial expansion approach up to third order in the fugacity. We find that the universal part of the third-order virial coefficient associated with two light atoms and one heavy atom is negative, while that associated with two heavy and one light atom changes sign from negative to positive as the mass ratio κ increases, and diverges when Efimov physics sets in at $\kappa = 13.61$. By examining the Helmholtz free energy, we find that the equilibrium polarization of the trapped and homogeneous systems is 0 for $\kappa = 1$, but finite for $\kappa \neq 1$ (with a majority of heavy particles). Compared to the equilibrium polarization of the non-interacting system, the equilibrium polarization at unitarity is increased for the trapped system and decreased for the homogeneous system. We find that unequal-mass Fermi gases are stable for all polarizations.

PACS numbers:

I. INTRODUCTION

It has been predicted that ultracold two-component Fermi gases with mismatching Fermi surfaces support novel phases such as the Fulde-Ferrell-Larkin-Ovchinnikov [1–3] state or other interesting phase separations, both in the homogeneous and inhomogeneous systems [4–9]. In equal-mass systems, the two Fermi surfaces differ if the number of fermions of species 1 and 2 differ, i.e., if the system exhibits a spin imbalance [10, 11]. Alternatively, mismatching Fermi surfaces arise if species 1 and 2 have different masses [12–19]. Experimentally, mass-imbalanced systems can be realized by simultaneously trapping, e.g., ⁶Li and ⁴⁰K [20–26]. The application of an external magnetic field in the vicinity of a Fano-Feshbach resonance allows for the realization of strongly-interacting gases, thus motivating our studies of the unequal-mass Fermi gas at unitarity.

At the few-body level, two-component unequal mass systems with short-range interspecies interactions and mass ratio κ are interesting because they support a variety of intriguing states [27]. At unitarity, the three-body system consisting of two heavy and one light particle [the $(n_1, n_2) = (2, 1)$ system] with zero-range interspecies interactions supports no three-body bound state in free space for $\kappa \leq 8.62$. For $8.62 \leq \kappa \leq 13.61$, however, the $(n_1, n_2) = (2, 1)$ system can support a bound state whose binding energy is determined by a three-body parameter [28–32]. For yet larger mass ratios ($\kappa > 13.61$), the three-body system in free space supports an infinite number of three-body Efimov states, which are geometrically spaced [33–35]. The spacing depends on the mass ratio κ between the heavy and light particles with the energy of the most deeply bound state being determined by the so-called three-body Efimov parameter [36].

The objective of this paper is to investigate the thermodynamics of inhomogeneous and homogeneous two-component Fermi gases as a function of the mass ratio κ .

Throughout, we consider the unitary regime where the interspecies s -wave scattering length diverges and determine the system properties as functions of the polarization P , $P = (N_1 - N_2)/(N_1 + N_2)$, and the temperature T . We are limiting ourselves to the so-called high temperature regime, where the virial equation of state up to the third order is expected to provide a valid description [37, 38]. For the trapped equal mass system, the virial equation of state up to the third order has been shown to be applicable over the temperature range of well above the Fermi temperature T_F down to about $T_F/2$ [39–43].

Our key findings are: (i) The second order virial equation of state in a harmonic trap is independent of the mass ratio κ . The mass ratio first enters at the third order in the virial expansion. (ii) The equilibrium state of the trapped system at unitarity is stable and favors a majority of heavy particles for $\kappa \neq 1$. (iii) The equation of state of the homogeneous system depends strongly on the mass ratio. The mass ratio first enters at the zeroth order in the virial expansion. (iv) The equilibrium state of the homogeneous system at unitarity is stable and favors a majority of heavy particles. The equilibrium polarization exhibits an intricate dependence on the third-order virial coefficients.

The paper is organized as follows. Section II defines the virial expansion and the first few virial expansion coefficients for a two-component Fermi gas in a harmonic trap where both species feel the same angular trapping frequency ω . The third order virial expansion coefficients at unitarity are determined as functions of the temperature and the mass ratio. Sections III and IV explore the virial equation of state of the harmonically trapped and homogeneous two-component Fermi gas at unitarity. Finally, Sec. V concludes. Appendix A summarizes the virial expansion for the harmonically trapped single-component Fermi gas and connects the results with those for the two-component Fermi gas.

II. DETERMINATION OF THE VIRIAL COEFFICIENTS

The model Hamiltonian $H(n_1, n_2)$ that describes unequal mass two-component Fermi gases with n_1 heavy and n_2 light particles in a harmonic trap with angular trapping frequency ω reads

$$H(n_1, n_2) = \sum_{j=1}^{n_1} \left(\frac{-\hbar^2}{2m_1} \vec{\nabla}_{\vec{r}_j}^2 + \frac{1}{2} m_1 \omega^2 r_j^2 \right) \quad (1)$$

$$+ \sum_{j=n_1+1}^{n_1+n_2} \left(\frac{-\hbar^2}{2m_2} \vec{\nabla}_{\vec{r}_j}^2 + \frac{1}{2} m_2 \omega^2 r_j^2 \right) + \sum_{i=1}^{n_1} \sum_{j=n_1+1}^{n_1+n_2} V_{tb}(r_{ij}),$$

where m_1 denotes the mass of the heavy species and m_2 denotes the mass of the light species. We define the mass ratio κ as $\kappa = m_1/m_2$ ($\kappa \geq 1$). In Eq. (1), \vec{r}_j denotes the position vector of the j^{th} atom measured with respect to the trap center. The interspecies interaction potential V_{tb} is parameterized by a zero-range potential, $V_{tb}(r_{ij}) = (2\pi\hbar^2 a_s / \mu_{red}) \delta(\vec{r}_{ij}) (\partial/\partial r_{ij}) r_{ij}$, where μ_{red} denotes the reduced mass, $\mu_{red} = m_1 m_2 / (m_1 + m_2)$, a_s the interspecies s -wave scattering length, and r_{ij} the interparticle distance, $r_{ij} = |\vec{r}_i - \vec{r}_j|$.

If the complete energy spectrum of the Hamiltonian given in Eq. (1) were known, one could calculate thermodynamic quantities like the average energy U or the entropy S from the free energy F , $F = -k_B T \ln Q_{n_1, n_2}$, using the canonical ensemble. Here, k_B is Boltzmann's constant and Q_{n_1, n_2} is the canonical partition function [44, 45],

$$Q_{n_1, n_2} = \text{Tr} \exp[-H(n_1, n_2)/(k_B T)], \quad (2)$$

where Tr is the trace operator. To evaluate the trace, we insert a complete set of eigenstates, yielding

$$Q_{n_1, n_2} = \sum_j \exp[-E_j^{(n_1, n_2)}/(k_B T)]. \quad (3)$$

The summation index j collectively denotes the complete set of quantum numbers allowed by symmetry.

In practice, it is easier to work in the grand canonical ensemble, which can be considered to be a collection of canonical ensembles with n_1 and n_2 particles of species 1 and 2 in thermal equilibrium with each other. In the grand canonical ensemble, the chemical potentials μ_1 and μ_2 of the two species are fixed. This implies that the system is characterized by the average numbers N_1 and N_2 of atoms of species 1 and 2. The thermodynamic potential $\Omega^{(2)}$ of the two-component Fermi gas in the grand canonical ensemble is [45]

$$\Omega^{(2)} = -k_B T \ln \text{Tr} \exp[-(H(n_1, n_2) - \mu_1 n_1 - \mu_2 n_2)/(k_B T)], \quad (4)$$

where the trace operator now extends over n_1 and n_2 . Rewritten in terms of the fugacities z_i , $z_i =$

$\exp[\mu_i/(k_B T)]$, the thermodynamic potential reads

$$\Omega^{(2)} = -k_B T \ln \left[\sum_{n_1=0}^{\infty} \sum_{n_2=0}^{\infty} Q_{n_1, n_2} z_1^{n_1} z_2^{n_2} \right]. \quad (5)$$

Throughout, we are interested in the large T limit where z_i is small. Taylor expanding Eq. (5) about $z_i = 0$ to third order, we find [41]

$$\Omega^{(2)} = \Omega_1^{(1)} + \Omega_2^{(1)} + \Delta\Omega, \quad (6)$$

where

$$\Omega_1^{(1)} = -k_B T Q_{1,0} \sum_{n_1=1}^{\infty} b_{n_1,0} z_1^{n_1}, \quad (7)$$

$$\Omega_2^{(1)} = -k_B T Q_{1,0} \sum_{n_2=1}^{\infty} b_{0, n_2} z_2^{n_2} \quad (8)$$

and

$$\Delta\Omega = -k_B T Q_{1,0} [b_{1,1} z_1 z_2 + b_{1,2} z_1 z_2^2 + b_{2,1} z_1^2 z_2 + \dots]. \quad (9)$$

Equations (6)-(9) show that the thermodynamic potential of the two-component Fermi gas can be written as a sum of the thermodynamic potentials $\Omega_1^{(1)}$ and $\Omega_2^{(1)}$ of components 1 and 2 and a correction term $\Delta\Omega$. The thermodynamic potentials $\Omega_1^{(1)}$ and $\Omega_2^{(1)}$ of the single-component species 1 and 2 are written in terms of the expansion or virial coefficients $b_{n_1,0}$ and b_{0, n_2} (see Appendix A) and the canonical partition function $Q_{1,0}$ of a single heavy particle of species 1. The $b_{n_1,0}$ (b_{0, n_2}) with $n_1 > 1$ ($n_2 > 1$) arise from the fermionic nature of the atoms and can be viewed as corrections to the Boltzmann gas [44, 45]. The correction term $\Delta\Omega$ contains the expansion or virial coefficients b_{n_1, n_2} , which account for the interactions between distinguishable fermions [46, 47],

$$b_{1,1} = (Q_{1,1} - Q_{1,0} Q_{0,1}) / Q_{1,0}, \quad (10)$$

$$b_{1,2} = (Q_{1,2} - Q_{1,0} Q_{0,2} - b_{1,1} Q_{1,0} Q_{0,1}) / Q_{1,0}, \quad (11)$$

and

$$b_{2,1} = (Q_{2,1} - Q_{2,0} Q_{0,1} - b_{1,1} Q_{1,0} Q_{1,0}) / Q_{1,0}. \quad (12)$$

In the non-interacting limit, i.e., for $a_s = 0$, we label the partition functions by a superscript NI. In this case, Q_{n_1, n_2}^{NI} reduces to $Q_{n_1,0} Q_{0, n_2}$, since $H(n_1, n_2)$ is separable for $a_s = 0$. In this limit, $b_{1,1}$ vanishes since $Q_{1,1}^{\text{NI}}$ equals $Q_{1,0} Q_{0,1}$. Consequently, $b_{1,2}$ and $b_{2,1}$ as well as all higher order virial coefficients b_{n_1, n_2} with $n_1 + n_2 > 3$ vanish; thus, $\Delta\Omega$ is zero for vanishing a_s .

To determine the b_{n_1, n_2} , one must know three things: (i) all $b_{i,j}$ where $i \leq n_1$ and $j < n_2$ or $i < n_1$ and $j \leq n_2$; (ii) all $Q_{i,0}$ and $Q_{0,j}$, where $i \leq n_1$ and $j \leq n_2$; and (iii) the complete energy spectrum of the (n_1, n_2) system. The $Q_{n_1,0}$ and Q_{0, n_2} characterize the single-component

Fermi gas and are calculated in Appendix A. In calculating the Q_{n_1, n_2} , it is convenient to express the total energy $E^{(n_1, n_2)}$ as a sum of the center of mass energy E_{CM} and the relative energy $E_{\text{rel}}^{(n_1, n_2)}$, $E^{(n_1, n_2)} = E_{\text{CM}} + E_{\text{rel}}^{(n_1, n_2)}$. In Eqs. (10)-(12), the center of mass contribution cancels the $Q_{1,0}$ term in the denominator [39].

We now evaluate the b_{n_1, n_2} at unitarity, i.e., for $1/a_s = 0$. The calculation of $b_{1,1}$ is straightforward [39]. The relative energies of the $(n_1, n_2) = (1, 1)$ system in a harmonic trap can be solved exactly using zero-range s -wave interactions [48]. The relative energies of the $(1, 1)$ system at unitarity are $E_{\text{rel}}^{(1,1)} = (2q + 1/2)\hbar\omega$ for $l = 0$ and $E_{\text{rel}}^{(1,1)} = (2q + l + 3/2)\hbar\omega$ for $l = 1, 2, \dots$, where q is a non-negative integer. As the relative energy spectrum for $l > 0$ is identical to the single particle energy spectrum, we have that $Q_{1,1}/Q_{1,0}$ is equal to $Q_{0,1}$ for states with $l > 0$. The remaining sum,

$$b_{1,1} = \sum_{q=0}^{\infty} \left(e^{-(2q+1/2)\tilde{\omega}} - e^{-(2q+3/2)\tilde{\omega}} \right), \quad (13)$$

includes all s -wave states and can be calculated analytically [39],

$$b_{1,1} = \frac{e^{\tilde{\omega}/2}}{1 + e^{\tilde{\omega}}}, \quad (14)$$

where $\tilde{\omega}$ denotes a dimensionless inverse temperature, $\tilde{\omega} = \hbar\omega/(k_B T)$. Equation (14) shows that $b_{1,1}$ is independent of the mass ratio. This is a direct consequence of the fact that the relative two-body energy spectrum is independent of the mass ratio. Furthermore, like the single-component virial coefficients b_n (see Appendix A), $b_{1,1}$ is an even function in $\tilde{\omega}$.

To calculate $b_{1,2}$ and $b_{2,1}$, we need the complete relative energy spectrum of the $(1, 2)$ system (1 light atom and 2 heavy atoms) and the $(2, 1)$ system (2 light atoms and 1 heavy atom), respectively. The three-body energies are conveniently expressed in terms of the quantity $\bar{\kappa}$,

$$\bar{\kappa} = \begin{cases} 1/\kappa & \text{for a majority of light species} \\ \kappa & \text{for a majority of heavy species.} \end{cases} \quad (15)$$

At unitarity, the relative three-body energies for inter-species s -wave zero-range interaction potentials can be written as $E_{\text{rel}}^{(n_1, n_2)} = (2q + s_{l, \nu} + 1)\hbar\omega$ [29], where $q = 0, 1, \dots$, and where the $s_{l, \nu}$ denote non-integer values. The $s_{l, \nu}$ depend on the particle symmetry and $\bar{\kappa}$, and are obtained by solving the five-dimensional hyperangular Schrödinger equation [49–51]. The hyperangular eigenvalues were first obtained for three identical bosons by Efimov [33], but have since been extended to any particle symmetry and mass ratio by both Efimov [34, 35] and others [49–51]. Application of Ref. [51] to the two-component system with $\bar{\kappa}$, relative angular momentum l ,

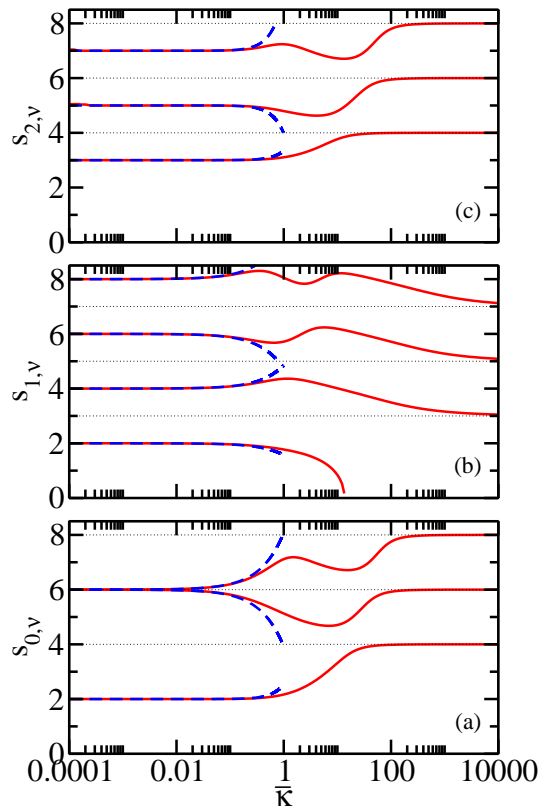


FIG. 1: (Color online) Hyperangular eigenvalues $s_{l, \nu}$ as a function of $\bar{\kappa}$ for (a) $l = 0$, (b) $l = 1$, and (c) $l = 2$ at unitarity. Note that $\bar{\kappa}$ is shown on a log scale. Solid lines show the $s_{l, \nu}$ obtained by solving Eq. (16), dashed lines show the limiting expressions, Eqs. (17)-(20), for $\bar{\kappa} \ll 1$, and thin dotted lines show the non-interacting $s_{l, \nu}^{\text{NI}}$.

and parity $(-1)^l$ at unitarity yields

$$-\frac{\sqrt{4\pi} \Gamma(l + 3/2)}{\Gamma\left(\frac{1+l-s_{l, \nu}}{2}\right) \Gamma\left(\frac{1+l+s_{l, \nu}}{2}\right)} = \left(\frac{-\bar{\kappa}}{\bar{\kappa} + 1}\right)^l \times \quad (16)$$

$${}_2F_1\left(1 + \frac{l - s_{l, \nu}}{2}, 1 + \frac{l + s_{l, \nu}}{2}, l + \frac{3}{2}, \frac{\bar{\kappa}^2}{(\bar{\kappa} + 1)^2}\right),$$

where Γ is the gamma function and ${}_2F_1$ is the hypergeometric function. Equation (16) has a spurious root at $s_{0, \nu} = 2$ for all $\bar{\kappa}$; this root needs to be removed “by hand”.

Solid lines in Fig. 1 show the $s_{l, \nu}$ as a function of $\bar{\kappa}$ for the three lowest relative angular momenta, i.e., for $l = 0, 1$, and 2 . The hyperangular quantum number ν , $\nu = 0, 1, \dots$, counts the number of times that the slope of $s_{l, \nu}$ changes sign. The thin dotted lines indicate the non-interacting limits, $s_{0, \nu}^{\text{NI}} = 2\nu + 4$ for $l = 0$ and $s_{l, \nu}^{\text{NI}} = 2\nu + l + 2$ for $l > 0$. The dashed lines show an expansion

of Eq. (16) for $\bar{\kappa} \ll 1$,

$$s_{0,0} \approx 2 + \frac{16}{3\pi^2} \bar{\kappa}^2, \quad (17)$$

$$s_{0,2j} \approx 4j + 2 + \frac{8}{\sqrt{3}\pi} \sqrt{j(j+1)} \bar{\kappa}, \quad (18)$$

$$s_{0,2j-1} \approx 4j + 2 - \frac{8}{\sqrt{3}\pi} \sqrt{j(j+1)} \bar{\kappa}, \quad (19)$$

where $j = 1, 2, \dots$, and

$$s_{l,\nu} \approx 2\nu + l + 1 + \frac{(-1)^{l+\nu} \Gamma(l+\nu+1)}{\sqrt{\pi} \Gamma(l+3/2) \Gamma(\nu+1)} \bar{\kappa}^l \quad (20)$$

for $l > 0$. For $l = 0$, the lowest eigenvalue varies quadratically with $\bar{\kappa}$ in the small $\bar{\kappa}$ regime. The higher lying $s_{l,\nu}$ values for $l = 0$ appear in pairs as $\bar{\kappa} \rightarrow 0$, with a splitting that is linear in $\bar{\kappa}$. For $l > 0$, in contrast, all eigenvalues are non-degenerate as $\bar{\kappa} \rightarrow 0$. The lowest $l = 1$ eigenvalue equals 2 for $\bar{\kappa} = 0$, crosses 1 for $\bar{\kappa} \approx 8.62$, and becomes purely imaginary for $\bar{\kappa} \approx 13.61$. The latter point indicates the onset of Efimov physics [28]. For $8.62 \leq \bar{\kappa} \leq 13.61$, non-universal three-body states can exist [28–32]. Similar behavior is found for the lowest $s_{l,\nu}$ values for higher odd angular momenta. The $s_{l,\nu}$ values for even l are greater than 1 for all $\bar{\kappa}$, indicating the absence of non-universal and Efimov physics in the even l angular momentum channels. For $l = 1, 3, 5, \dots$ [see Fig. 1(b) for $l = 1$], the $s_{l,\nu}$ with $\nu > 0$ begin one unit below the non-interacting value in the $\bar{\kappa} = 0$ limit and decrease to the next lower non-interacting value in the limit $\bar{\kappa} \rightarrow \infty$. For $l = 2, 4, 6, \dots$ [see Fig. 1(c) for $l = 2$], the $s_{l,\nu}$ begin one unit below the non-interacting values in the $\bar{\kappa} = 0$ limit and approach the non-interacting values in the limit $\bar{\kappa} \rightarrow \infty$. In the limit $\bar{\kappa} \rightarrow \infty$, all states save those that describe Efimov physics behave like non-interacting states. The two masses are so heavy compared to the single light particle that even infinitely strong interactions cannot mediate a lowering of the energy.

Now that we have the $s_{l,\nu}$, we can calculate $Q_{1,2}$ and $Q_{2,1}$, and thus $b_{1,2}$ and $b_{2,1}$. We restrict ourselves to the regime where Efimov physics is absent (i.e., we limit ourselves to $\bar{\kappa} \leq 13.61$) and we assume that the three-body system behaves fully universal (i.e., we assume the absence of three-body resonances in the regime $8.62 \leq \bar{\kappa} \leq 13.61$). Under these assumptions, the virial coefficient $b_{2,1}$, Eq. (12), can be written as

$$b_{2,1} = \sum_{l=0}^{\infty} b_{2,1}(l), \quad (21)$$

where

$$b_{2,1}(l) = \sum_{\nu=0}^{\infty} \sum_{q=0}^{\infty} (2l+1) \left[e^{-(2q+s_{l,\nu}+1)\tilde{\omega}} - e^{-(2q+s_{l,\nu}^{\text{NI}}+1)\tilde{\omega}} - e^{-(2q+1/2+2\nu+l+3/2)\tilde{\omega}} + e^{-(2q+3/2+2\nu+l+3/2)\tilde{\omega}} \right]. \quad (22)$$

The first and second terms in the square bracket on the right hand side of Eq. (22) arise from the $Q_{2,1}/Q_{1,0}$ and $Q_{2,0}$ terms, respectively, while the third and fourth terms in the square bracket on the right hand side of Eq. (22) arise from the $-b_{1,1}Q_{1,0}$ term. For $l > 0$, the second and fourth terms cancel, while the third term can be rewritten in terms of $s_{l,\nu}^{\text{NI}}$. Performing the sum over q analytically, we find

$$b_{2,1}(l > 0) = \frac{e^{2\tilde{\omega}}}{e^{2\tilde{\omega}} - 1} \times \left[(2l+1) \sum_{\nu=0}^{\infty} \left(e^{-(s_{l,\nu}+1)\tilde{\omega}} - e^{-s_{l,\nu}^{\text{NI}}\tilde{\omega}} \right) \right]. \quad (23)$$

For $l = 0$, the second and fourth terms do not completely cancel and contribute, after the sum over q is done analytically, a term proportional to $\exp(-3\tilde{\omega})$. Combining the first and third terms in the square bracket on the right hand side of Eq. (22), we find

$$b_{2,1}(l = 0) = \frac{e^{2\tilde{\omega}}}{e^{2\tilde{\omega}} - 1} \left[e^{-3\tilde{\omega}} - e^{-2\tilde{\omega}} + \sum_{\nu=0}^{\infty} \left(e^{-(s_{0,\nu}+1)\tilde{\omega}} - e^{-s_{0,\nu}^{\text{NI}}\tilde{\omega}} \right) \right]. \quad (24)$$

Since the mass ratio dependence only enters through the $s_{l,\nu}$, Eqs. (21)-(24) remain valid for $b_{1,2}$. In practice, we calculate the first 10,000 $s_{l,\nu}$ values for each l , $l = 0 - 50$, and determine the $b_{1,2}(l)$ and $b_{2,1}(l)$ using Eqs. (23) and (24). We find that we obtain better convergence if we employ the same cutoff on the terms that involve $s_{l,\nu}$ and $s_{l,\nu}^{\text{NI}}$ than if we perform the sum over ν that involves the non-interacting $s_{l,\nu}^{\text{NI}}$ values analytically.

Figure 2 shows the $b_{2,1}(l)$ for the first five angular momenta for (a) $\bar{\kappa} = 1$ and (b) $\bar{\kappa} = 6.67$. The $b_{2,1}(l)$ are negative for even l and positive for odd l for all $\tilde{\omega}$. The leading contribution for any mass ratio comes from the solution with $\nu = 0$. For odd l , we have $s_{l,0} + 1 < s_{l,0}^{\text{NI}}$ [see Fig. 1(b) for $l = 1$], implying that the $b_{2,1}(l)$ are positive for all $\tilde{\omega}$ and $\bar{\kappa}$. For even l , we have $s_{l,0} + 1 > s_{l,0}^{\text{NI}}$ [see Fig. 1(c) for $l = 2$], implying that the $b_{2,1}(l)$ are negative. For $l = 0$, the $-\exp(-2\tilde{\omega})$ term gives the leading contribution, implying that $b_{2,1}(l)$ is negative for all $\tilde{\omega}$ and $\bar{\kappa}$. A similar analysis can be conducted for the $b_{1,2}(l)$. The alternating sign of the $b_{1,2}(l)$ and the $b_{2,1}(l)$ implies that the full virial coefficients $b_{1,2}$ and $b_{2,1}$ converge like an alternating series as more l terms are included. We find that the convergence rate decreases as $\bar{\kappa}$ increases.

Figure 3 shows the virial coefficients $b_{2,1}$ for $\bar{\kappa} = 2, 3, 4$ and 6.67 (from bottom to top) as a function of $\tilde{\omega}$. The virial coefficient $b_{2,1}$ for $\bar{\kappa} = 2$ and 3 is negative for all $\tilde{\omega}$. The virial coefficient for $\bar{\kappa} = 4$ is negative for large $\tilde{\omega}$, changes sign at $\tilde{\omega} \approx 1.67$, and is positive for small $\tilde{\omega}$. The virial coefficient for $\bar{\kappa} = 6.67$ changes sign at a much lower temperature, i.e., at $\tilde{\omega} \approx 5.59$. The sign change of $b_{2,1}$ can be attributed to the fact that the negative $l = 0$ contribution increases slower in magnitude than the positive $l = 1$ contribution with increasing $\bar{\kappa}$ (see Fig. 2), so

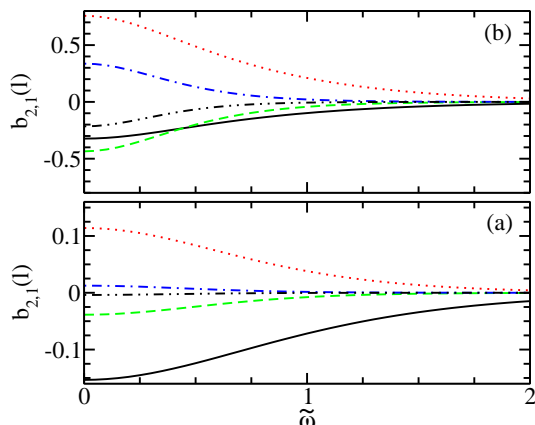


FIG. 2: (Color online) Angular momentum contributions $b_{2,1}(l)$ for $l = 0 - 4$ for (a) $\bar{\kappa} = 1$ and (b) $\bar{\kappa} = 6.67$ as a function of $\tilde{\omega}$ at unitarity. Solid, dotted, dashed, dash-dotted, and dash-dot-dotted lines show $b_{2,1}(l)$ for $l=0, 1, 2, 3,$ and 4 , respectively.

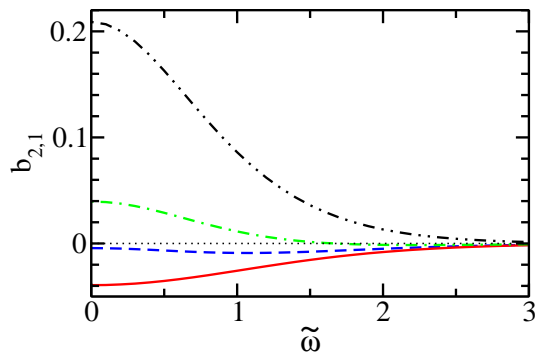


FIG. 3: (Color online) Solid, dashed, dash-dotted, and dash-dot-dotted lines show the virial coefficient $b_{2,1}$ as a function of $\tilde{\omega}$ for $\bar{\kappa} = 2, 3, 4$ and 6.67 . The thin dotted line at 0 is a guide to emphasize the sign change of $b_{2,1}$ for $\bar{\kappa} = 4$ around $\tilde{\omega} \approx 1.67$.

that the positive $l = 1$ contribution dominates for sufficiently large $\bar{\kappa}$. In the high temperature limit, $b_{2,1}$ first becomes positive for $\bar{\kappa} \approx 3.11$. In the low temperature regime, $b_{2,1}$ remains negative for $\bar{\kappa} < 8.62$ and changes sign when $s_{1,0} = 1$, i.e., the $\bar{\kappa}$ value beyond which three-body resonances can appear [28–32]. We find that the virial coefficient $b_{1,2}$ is negative for all $\bar{\kappa}$ and $\tilde{\omega}$. We note that a general framework for calculating $b_{1,2}$ and $b_{2,1}$ for unequal-mass systems is given in Ref. [52]; however, this reference did not provide numerical values for $b_{1,2}$ and $b_{2,1}$. The fact that the third order virial coefficient $b_{2,1}$

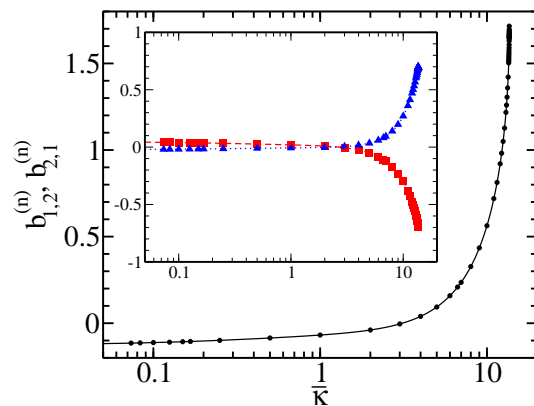


FIG. 4: (Color online) Circles show the universal parts $b_{1,2}^{(0)}$ ($\bar{\kappa} < 1$) and $b_{2,1}^{(0)}$ ($\bar{\kappa} > 1$) of the virial coefficients as a function of $\bar{\kappa}$. The inset (the axes use the same labels as the main panel) shows the first non-universal corrections $b_{1,2}^{(2)}$ and $b_{2,1}^{(2)}$ (squares) and the second non-universal corrections $b_{1,2}^{(4)}$ and $b_{2,1}^{(4)}$ (triangles) as a function of $\bar{\kappa}$. The lines are guides to the eye.

changes sign as $\bar{\kappa}$ increases suggests that the higher order virial coefficients might also change sign. Throughout this paper, we restrict our analysis to systems with $n_1 + n_2 \leq 3$.

In the high temperature limit, we Taylor expand the b_{n_1, n_2} ($n_1 + n_2 = 3$) [53],

$$b_{n_1, n_2} = b_{n_1, n_2}^{(0)} + b_{n_1, n_2}^{(2)} \tilde{\omega}^2 + b_{n_1, n_2}^{(4)} \tilde{\omega}^4 + \dots \quad (25)$$

To our calculated accuracy, we find that the odd powers vanish, i.e., the virial coefficients $b_{1,2}$ and $b_{2,1}$ appear to be even functions in $\tilde{\omega}$, similar to their single-component counterparts. For the equal-mass system, the expression (25) was considered in Ref. [39]. The $b_{n_1, n_2}^{(0)}$ term is independent of $\tilde{\omega}$ and thus universal. The higher order corrections $b_{1,2}^{(n>0)}$ and $b_{2,1}^{(n>0)}$ are non-universal, since they depend on the harmonic trapping potential through $\tilde{\omega}$. The supplementary material [53] tabulates the $b_{1,2}^{(n)}$ and $b_{2,1}^{(n)}$, $n = 0, 2, 4$ and 6 , as a function of $\bar{\kappa}$. The $b_{1,2}^{(n)}$ and $b_{2,1}^{(n)}$ with $n = 0, 2,$ and 4 are shown in Fig. 4 as a function of $\bar{\kappa}$, where $\bar{\kappa}$ is shown on a log scale. The universal virial coefficient $b_{2,1}^{(0)}$ has an infinite slope at $\bar{\kappa} = 13.61$ where Efimov physics sets in. For $\bar{\kappa} > 13.61$ (not shown), $b_{2,1}^{(0)}$ is expected to diverge due to the contributions of the infinite sequence of Efimov trimers. In the limit $\bar{\kappa} \rightarrow 0$,

the $b_{1,2}(l)$ with $l > 0$ vanish and we have

$$b_{1,2}(\bar{\kappa} = 0) = \frac{-e^{2\tilde{\omega}}}{(e^{\tilde{\omega}} + 1)^2(e^{2\tilde{\omega}} + 1)} \approx -\frac{1}{8} + \frac{3}{32}\tilde{\omega}^2 - \frac{3}{64}\tilde{\omega}^4 + \mathcal{O}(\tilde{\omega}^6). \quad (26)$$

III. THERMODYNAMICS OF THE TRAPPED MASS-IMBALANCED TWO-COMPONENT FERMI GAS

This section considers the thermodynamics of the harmonically trapped two-component Fermi gas at unitarity as a function of κ . For the equal-mass case, we refer the reader to Refs. [39–43]. We measure our temperature T in units of the semi-classical Fermi temperature T_F of a single-component Fermi gas with $N/2$ particles of mass m_1 , $T_F = [6(N/2)]^{1/3}\hbar\omega/k_B$ [54]. Correspondingly, our energy is measured in units of E_F , where $E_F = k_B T_F$. Our starting point is the thermodynamic potential $\Omega^{(2)}$, Eq. (6), with $n_1 + n_2 \leq 3$ (i.e., including $b_{1,1}$, $b_{1,2}$, and $b_{2,1}$).

The two coupled number equations, derived from $N_i = -\partial\Omega^{(2)}/\partial\mu_i$ ($i = 1$ and 2), are

$$\frac{N_1}{Q_{1,0}} = f_1(z_1) + b_{1,1}z_1z_2 + 2b_{2,1}z_1^2z_2 + b_{1,2}z_1z_2^2 \quad (27)$$

and

$$\frac{N_2}{Q_{1,0}} = f_2(z_2) + b_{1,1}z_1z_2 + b_{2,1}z_1^2z_2 + 2b_{1,2}z_1z_2^2. \quad (28)$$

Throughout, we use the full temperature dependent expressions for the virial coefficients, and

$$f_1(z_1) = \sum_{n_1=0}^{\infty} n_1 b_{n_1,0} z_1^{n_1} \quad (29)$$

and

$$f_2(z_2) = \sum_{n_2=0}^{\infty} n_2 b_{0,n_2} z_2^{n_2}. \quad (30)$$

Equations (29) and (30) can be employed if $z_i < e^{3\tilde{\omega}/2}$, $i = 1, 2$. For larger z_i , useful parameterizations of Eqs. (29) and (30) are

$$f_i(z_i) \approx -\text{Li}_3(-z_i) + \frac{1}{8}\tilde{\omega}^2 [-\text{Ln}(1+z_i) - \text{Li}_3(-z_i)] + \frac{1}{1920}\tilde{\omega}^4 \left[\frac{17z_i}{(1+z_i)^2} - 30\text{Ln}(1+z_i) - 13\text{Li}_3(-z_i) \right] + \mathcal{O}(\tilde{\omega}^6), \quad (31)$$

where Ln is the natural logarithm function and Li is the polylogarithm function. For the temperatures considered

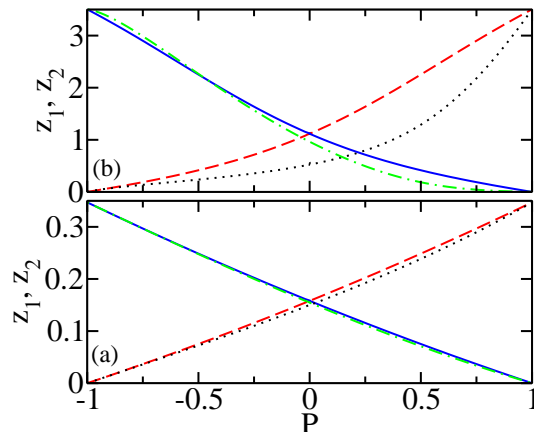


FIG. 5: (Color online) Trapped system at unitarity. Solid and dashed lines (dash-dotted and dotted lines) show the fugacities z_1 and z_2 , respectively, for $\kappa = 1$ ($\kappa = 13$) as a function of the polarization P for $N = 5 \times 10^7$ and (a) $T/T_F = 1$ and (b) $T/T_F = 1/2$.

in this paper, terms of order $\tilde{\omega}^6$ and higher are negligible. Equations (29) and (30) treat the non-interacting “reference pieces” $f_1(z_1)$ and $f_2(z_2)$ as an infinite series in the fugacities and the interacting pieces at third order in the fugacities. Alternatively, one may consider truncating the non-interacting and interacting pieces at the same order in the fugacities. We have opted for the former approach for two reasons: (i) In the limit that $P = 1$ or -1 , we recover the exact results of the single-component Fermi gas. (ii) In the regime where the z_i are small, i.e., in the regime where the virial equation of state up to third order is expected to provide reliable results, we find fairly small differences [e.g., $< 0.06\%$ in Fig. 5(a)] between the approaches that treat the non-interacting piece at infinite order and third order in the fugacities. For a given temperature T , polarization P , and total number of particles N , we solve Eqs. (27) and (28) self-consistently for z_1 and z_2 .

Figure 5 shows the fugacities z_1 and z_2 at unitarity as a function of the polarization for (a) $T/T_F = 1$ and (b) $T/T_F = 1/2$ for $\kappa = 1$ (solid and dashed lines) and $\kappa = 13$ (dash-dotted and dotted lines). The fugacities for $T/T_F = 1$ are smaller than 0.35 for both mass ratios considered, suggesting that the virial equation of state can likely be trusted for $T/T_F \geq 1$. For $T/T_F = 1/2$, in contrast, the fugacities are as large as 3.5, suggesting that the description is at best qualitatively correct. On the scale shown, the fugacities for $T/T_F = 1$ and $\kappa = 1$ are nearly indistinguishable from those at the same temperature but higher mass ratio. This makes sense intuitively, since the fugacities are small in the high temperature regime, thereby suppressing higher order terms in the

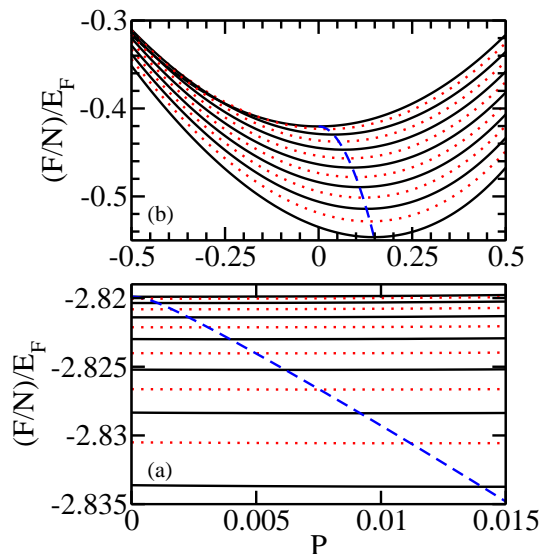


FIG. 6: (Color online) Free energy per particle F/N ($N = 5 \times 10^7$) as a function of the polarization P for (a) $T/T_F = 1$ and (b) $T/T_F = 1/2$ for the trapped system at unitarity. Alternating solid and dotted curves, from top to bottom, show the free energy for $\kappa = 1 - 13$ in units of 1. The dashed lines connect the (F_{eq}, P_{eq}) points for different κ .

virial expansion. At lower temperatures [see Fig. 5(b)], the higher order virial coefficients become more important, as evidenced by the fact that the fugacities show a notable dependence on the mass ratio.

In the following, we use the virial equation of state to determine the free energy F , $F = \Omega^{(2)} + \mu_1 N_1 + \mu_2 N_2$, the entropy S , $S = -\partial \Omega^{(2)} / \partial T$ (calculated for fixed ω , μ_1 and μ_2), and the energy U , $U = F + TS$, as a function of the mass ratio κ , the polarization P , and the temperature T at unitarity. Solid and dotted lines in Fig. 6 show the free energy per particle F/N as a function of the polarization for (a) $T/T_F = 1$ and (b) $T/T_F = 1/2$. In both panels, the alternating solid and dotted lines, from top to bottom, correspond to mass ratios $\kappa = 1, 2, \dots, 13$. For the equal mass system, the minimum of the free energy occurs for $P = 0$, i.e., for equal numbers of spin-up and spin-down fermions. As κ increases, the minimum of the free energy moves to positive polarizations, i.e., to a majority of heavy particles. We refer to the (F, P) values at which the free energy is minimized as (F_{eq}, P_{eq}) . Dashed lines in Figs. 6(a) and 6(b) connect the (F_{eq}, P_{eq}) values for different κ . For both temperatures, P_{eq} increases with increasing κ , which can be understood by realizing that the three-body system consisting of two heavy atoms and one light atom has a lower energy than the three-body system consisting of one heavy atom and two light atoms. Moreover, for a given κ , P_{eq} increases with decreasing temperature. This trend makes sense, since

we expect interaction effects to become more important as the temperature decreases.

To obtain an analytical expression for P_{eq} , we take the derivative of F with respect to P at fixed temperature and fixed number of particles. We find that the extremum of P occurs when the two fugacities are equal (i.e., $z_1 = z_2 = z_{eq}$). This restriction allows for a straightforward calculation of z_{eq} , namely

$$\frac{N}{Q_{1,0}} = f_1(z_{eq}) + f_2(z_{eq}) + 2b_{1,1}z_{eq}^2 + 3(b_{2,1} + b_{1,2})z_{eq}^3 \quad (32)$$

can be solved self-consistently for fixed N and T . Up to third order in z_{eq} , P_{eq} can be written as

$$P_{eq} = \frac{N}{Q_{1,0}}(b_{2,1} - b_{1,2})z_{eq}^3. \quad (33)$$

P_{eq} is equal to zero for all κ if the virial equation of state terminates at the second order in the fugacity. At the third order, we find $P_{eq} = 0$ for $\kappa = 1$, since $b_{1,2}$ equals $b_{2,1}$ in this case. For $\kappa > 1$, however, P_{eq} is positive since $b_{2,1} > b_{1,2}$ for all $\kappa > 1$. Interestingly, the sign change of $b_{2,1}$ in the high temperature regime for $\kappa \approx 3.11$ does not lead to a discontinuity or a sign change of P_{eq} since $b_{1,2}$ is finite and negative for all κ . For small deviations from $\kappa = 1$, we find that P_{eq} and F_{eq} change linearly and quadratically, respectively, as a function of κ for fixed temperature and fixed number of particles. We find that $\partial^2 F / \partial P^2$, calculated for fixed T and N , is greater than zero for all polarizations and mass ratios considered, which implies that the system is stable at this level of approximation.

To discuss the dependence of the entropy S and the energy U on the temperature and the polarization, we focus on the mass ratio $\kappa = 6.67$, i.e., on the experimentally realizable K-Li system at unitarity [20–26]. Thin dotted and solid lines in Fig. 7(a) show the free energy per particle as a function of the polarization for $T/T_F = 1, 1.2, \dots, 1.8$ (from top to bottom). The dashed line connects the (F_{eq}, P_{eq}) values for different T (but fixed κ and N). The vertical solid line marks the value P_{eq} for $T/T_F = 1$, where $F/N = -2.82E_F$, $S/N = 5.73k_B$, and $U/N = 2.91E_F$. Thin solid and dotted lines in Fig. 7(b) show the entropy per particle S/N as a function of the polarization for $T/T_F = 0.95, 0.96, \dots, 1.04$ (from bottom at $P \approx 0$ to top at $P \approx 0.5$). Similarly, thin solid and dotted lines in Fig. 7(c) show the energy per particle U/N as a function of the polarization for $T/T_F = 0.99, 1, \dots, 1.06$ (from bottom at $P \approx 0.5$ to top at $P \approx 0.1$). The dashed lines in Figs. 7(b) and 7(c) connect points of constant $U/N = 2.91E_F$ and $S/N = 5.73k_B$, respectively (i.e., the values of U/N and S/N at P_{eq} for $T/T_F = 1$). As expected, the entropy for a fixed energy and the energy for a fixed entropy are concave and convex functions of the polarization, respectively. It can be seen that the entropy per particle S/N is maximized at P_{eq} while the energy per particle U/N is minimized at P_{eq} . The fact

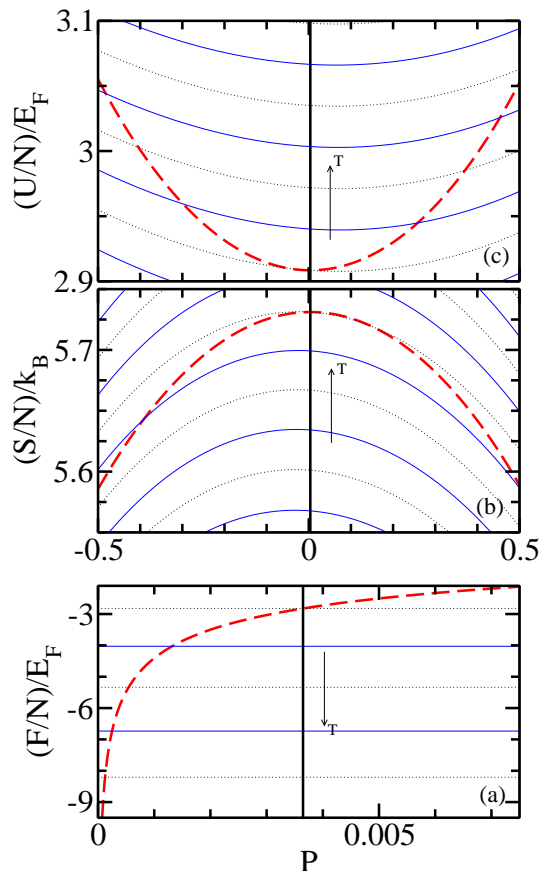


FIG. 7: (Color online) Thermodynamic observables F/N , S/N , and U/N as a function of the polarization P for $\kappa = 6.67$ and $N = 5 \times 10^7$ for the trapped system at unitarity. Alternating dotted and solid lines show (a) the free energy per particle F/N for $T/T_F = 1, 1.2, \dots, 1.8$ (from top to bottom), (b) the entropy per particle S/N for $T/T_F = 0.95, 0.96, \dots, 1.04$ (from bottom at $P \approx 0$ to top at $P \approx 0.5$), and (c) the energy per particle U/N for $T/T_F = 0.99, 1, \dots, 1.06$ (from bottom at $P \approx 0.5$ to top at $P \approx 0.1$). In panel (a), the dashed line connects (F_{eq}, P_{eq}) values for different T . In panels (b) and (c), the dashed lines show S/N for $U/N = 2.91E_F$ and U/N for $S/N = 5.73k_B$, respectively. In all three panels, the vertical lines indicate the value of P_{eq} for $T/T_F = 1$.

that $-\partial^2 S/\partial P^2$ ($\partial^2 U/\partial P^2$) is greater than zero for fixed U and N (for fixed S and N) is consistent with the fact that the system is stable as concluded earlier from the fact that $\partial^2 F/\partial P^2$ is greater than zero for fixed T and N . Lastly, we note that the maximum of the isotherm S/N moves to smaller P with decreasing T and that the minimum of the isotherm U/N moves to larger P with decreasing T .

The thermodynamic quantities shown in Figs. 5-7 have been obtained for $N = 5 \times 10^7$ particles. For fixed T/T_F , the actual temperature T decreases with decreasing N ,

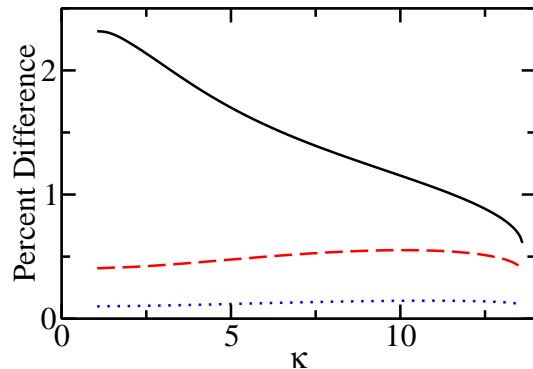


FIG. 8: (Color online) Percent difference between P_{eq} for $N = 5 \times 10^7$ and P_{eq} for $N = 500$ as a function of the mass ratio κ for the trapped system at unitarity. Solid, dashed and dotted lines show the percent difference for $T/T_F = 1/2, 1$ and 2 , respectively.

since T_F decreases with decreasing N . Correspondingly, $\tilde{\omega}$ increases with decreasing N (again, assuming fixed T/T_F). Since the leading order non-universal corrections scale with $\tilde{\omega}^2$ [see Eqs. (25) and (31)], the non-universal corrections are expected to be negligible for large N , but not for very small N . Figure 8 shows the percentage difference between P_{eq} for $N = 5 \times 10^7$ and P_{eq} for $N = 500$ as a function of κ for $T/T_F = 2, 1$ and $1/2$. The non-universal corrections are largest, i.e., on the order of 2%, for $\kappa = 1$ and $T/T_F = 1/2$ [solid line in Fig. 8]. For larger N , the non-universal corrections are even smaller, implying that Figs. 5-7 show essentially universal, N -independent thermodynamic quantities of the trapped two-component Fermi system with equal trapping frequencies.

We conclude this section by noting that P_{eq} is quite small for the K-Li system down to $T/T_F = 1$, but then changes more rapidly as the temperature is lowered further. The dependence of P_{eq} on the mass ratio κ may be enhanced by switching to a trap geometry for which the single-particle energies are dependent on the mass m_1 or m_2 . One such system is, as detailed in the next section, the homogeneous system, which favors much larger polarizations than the trapped system for comparable T/T_F .

IV. THERMODYNAMICS OF THE UNIVERSAL HOMOGENEOUS MASS-IMBALANCED TWO-COMPONENT FERMION GAS

A. Local Density Approximation

This section shows how the homogeneous system can be related to the harmonically trapped system via the local density approximation [39, 55]. In the high tem-

perature limit, the thermodynamic potential $\Omega_{\text{hom}}^{(2)}$ of the homogeneous system can be written as

$$\Omega_{\text{hom}}^{(2)} = \Omega_{1,\text{hom}}^{(1)} + \Omega_{2,\text{hom}}^{(1)} + \Delta\Omega_{\text{hom}}, \quad (34)$$

where

$$\Omega_{1,\text{hom}}^{(1)} = -k_B T \frac{V}{\lambda_{m_1}^3} \sum_{n_1=1}^{\infty} b_{n_1,0,\text{hom}} z_1^{n_1}, \quad (35)$$

$$\Omega_{2,\text{hom}}^{(1)} = -k_B T \frac{V}{\lambda_{m_1}^3} \sum_{n_2=1}^{\infty} b_{0,n_2,\text{hom}} z_2^{n_2}, \quad (36)$$

and

$$\Delta\Omega_{\text{hom}} = -k_B T \frac{V}{\lambda_{m_1}^3} \sum_{n_1=1}^{\infty} \sum_{n_2=1}^{\infty} b_{n_1,n_2,\text{hom}} z_1^{n_1} z_2^{n_2}. \quad (37)$$

Here, the $b_{n_1,n_2,\text{hom}}$ denote the virial coefficients of the homogeneous system, and z_1 and z_2 are the fugacities of the homogeneous system. The virial coefficients $b_{n_1,n_2,\text{hom}}$ are defined by Eqs. (10)-(12) with the Q_{n_1,n_2} interpreted as the partition functions of the homogeneous systems. Equations (34)-(37) are analogous to the high temperature limits of Eqs. (6)-(9). In Eqs. (34)-(37), we used that the high temperature limit of $Q_{1,0,\text{hom}}$ is given by $V/\lambda_{m_1}^3$ [45], where V is the volume of the system and where λ_{m_1} is the thermal de Broglie wavelength of a particle of the heavy species,

$$\lambda_{m_1} = \sqrt{\frac{2\pi\hbar^2}{m_1 k_B T}}. \quad (38)$$

In the local density approximation [39, 55], the thermodynamic potential $\Omega^{(2)}$ of the trapped system is given by a weighted average of $\Omega_{\text{hom}}^{(2)}(\vec{r})$ over all space,

$$\Omega^{(2)} = \frac{\int \Omega_{\text{hom}}^{(2)}(\vec{r}) d^3\vec{r}}{\int d^3\vec{r}}, \quad (39)$$

i.e., we assume that the thermodynamic potential at each location \vec{r} in the trap can be approximated by the corresponding bulk value. This implies that the z_i in Eqs. (35)-(37) are replaced by $z_i(\vec{r})$, $z_i(\vec{r}) = \exp[\mu_{i,\text{loc}}(\vec{r})/(k_B T)]$, where the local chemical potentials $\mu_{i,\text{loc}}(\vec{r})$ are defined as

$$\mu_{i,\text{loc}}(\vec{r}) = \mu_i - \frac{1}{2} m_i \omega^2 r^2. \quad (40)$$

The integrations on the right hand side of Eq. (39) are straightforward. We first perform the integration involving $\Delta\Omega_{\text{hom}}(\vec{r})$. The integration in the denominator introduces a factor of V , which cancels with the factor of V in the numerator. This leaves, after performing the angular integrals,

$$\Delta\Omega = -4\pi \frac{k_B T}{\lambda_{m_1}^3} \sum_{n_1=1}^{\infty} \sum_{n_2=1}^{\infty} b_{n_1,n_2,\text{hom}} z_1^{n_1} z_2^{n_2} \times \int_0^{\infty} \exp[-\frac{1}{2}(m_1 n_1 + m_2 n_2)\omega^2 r^2 / (k_B T)] r^2 dr. \quad (41)$$

Performing the remaining integration and expressing the result in terms of the mass ratio κ , we find

$$\Delta\Omega = -k_B T \left(\frac{k_B T}{\hbar\omega} \right)^3 \times \sum_{n_1=1}^{\infty} \sum_{n_2=1}^{\infty} \frac{b_{n_1,n_2,\text{hom}}}{(n_1 + n_2/\kappa)^{3/2}} z_1^{n_1} z_2^{n_2}. \quad (42)$$

The prefactor $[k_B T/(\hbar\omega)]^3$ coincides with the high T limit of $Q_{1,0}$ for the trapped system. Comparison of Eqs. (9) and (42) allows us to relate the universal virial coefficients $b_{n_1,n_2}^{(0)}$ of the trapped system to the virial coefficients $b_{n_1,n_2,\text{hom}}$ of the homogeneous system,

$$b_{n_1,n_2,\text{hom}} = (n_1 + n_2/\kappa)^{3/2} b_{n_1,n_2}^{(0)}. \quad (43)$$

Considering the integrations over $\Omega_{1,\text{hom}}^{(1)}(\vec{r})$ and $\Omega_{2,\text{hom}}^{(1)}(\vec{r})$, one finds analogous relationships between $b_{n_1,0,\text{hom}}$ and $b_{n_1,0}^{(0)}$, and between $b_{0,n_2,\text{hom}}$ and $b_{0,n_2}^{(0)}$.

B. Universal thermodynamics of the homogeneous system

This section considers the universal, N -independent thermodynamics of the homogeneous two-component Fermi gas at unitarity as a function of κ . We measure our temperature T in units of the semi-classical Fermi temperature T_F of a single-component Fermi gas with $N/2$ particles of mass m_1 , $k_B T_F = [6\pi^2(N/2)/V]^{2/3} \hbar^2 / (2m_1)$ [45]. Notice that the Fermi temperature scales inversely with the mass m_1 . This implies that the Fermi temperature of $N/2$ light particles with mass m_2 is κ times larger than the Fermi temperature of $N/2$ heavy particles. The different Fermi temperatures of the single-component heavy and light particles are, of course, a direct consequence of the mismatching Fermi surfaces of unequal-mass Fermi gases or, equivalently, a direct consequence of the fact that the single-particle energies of a mass m_i particle in a box with periodic boundary conditions scale with $1/m_i$. The high temperature virial equation of state of the homogeneous system can be applied down to T/T_F about 1 for $\kappa = 1$. For unequal masses, the applicability regime, using the heavy mass to define T_F (see above), is limited to $T/T_F \gtrsim \kappa$.

The coupled number equations of the homogeneous system, up to third order, read

$$\frac{N_1 \lambda_{m_1}^3}{V} = -\text{Li}_{3/2}(-z_1) + b_{1,1,\text{hom}} z_1 z_2 + 2b_{2,1,\text{hom}} z_1^2 z_2 + b_{1,2,\text{hom}} z_1 z_2^2 \quad (44)$$

and

$$\kappa^{3/2} \frac{N_2 \lambda_{m_1}^3}{V} = -\text{Li}_{3/2}(-z_2) + \kappa^{3/2} b_{1,1,\text{hom}} z_1 z_2 + \kappa^{3/2} b_{2,1,\text{hom}} z_1^2 z_2 + 2\kappa^{3/2} b_{1,2,\text{hom}} z_1 z_2^2. \quad (45)$$

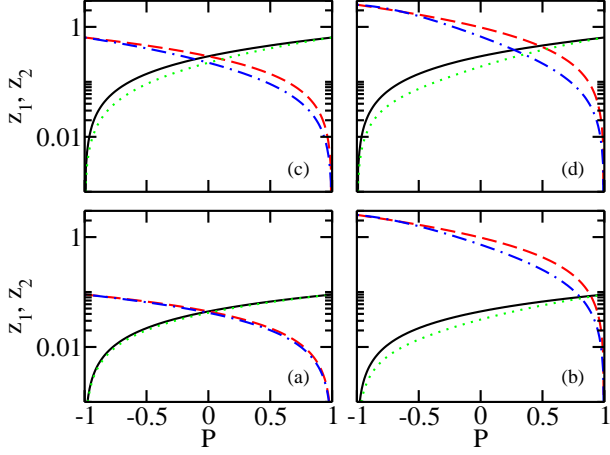


FIG. 9: (Color online) Fugacities z_1 and z_2 of the homogeneous system as a function of the polarization P for (a) $\kappa = 1$ and $T/T_F = 6.67$, (b) $\kappa = 6.67$ and $T/T_F = 6.67$, (c) $\kappa = 1$ and $T/T_F = 2$, and (d) $\kappa = 2$ and $T/T_F = 2$. Dotted and dash-dotted lines show z_1 and z_2 , respectively, for the unitary system obtained by solving Eqs. (44) and (45) self-consistently. For comparison, solid and dashed lines show z_1 and z_2 , respectively, for the non-interacting system.

Dotted and dash-dotted lines in Fig. 9 show z_1 and z_2 , respectively, as a function of the polarization P for the unitary system obtained by solving Eqs. (44) and (45) self-consistently for fixed κ and T . The panels show the fugacities for (a) $\kappa = 1$ and $T/T_F = 6.67$, (b) $\kappa = 6.67$ and $T/T_F = 6.67$, (c) $\kappa = 1$ and $T/T_F = 2$, and (d) $\kappa = 2$ and $T/T_F = 2$. For the equal mass case, Eqs. (44) and (45) are symmetric and thus z_1 and z_2 are symmetric about $P = 0$ for any temperature [see Figs. 9(a) and 9(c)]. For unequal masses, in contrast, Eqs. (44) and (45) are not symmetric and the crossing of the fugacities z_1 and z_2 is shifted to positive polarizations [see Figs. 9(b) and 9(d)]. For comparison, solid and dashed lines in Fig. 9 show the fugacities z_1 and z_2 , respectively, for the corresponding non-interacting systems. Even for the non-interacting system, the fugacities z_1 and z_2 are not symmetric with respect to $P = 0$; this is a direct consequence of the $\kappa^{3/2}$ factor in Eq. (45). For $-1 < P < 1$, the fugacities for the non-interacting systems lie above the respective fugacities for the unitary systems. For $\kappa > 1$, this implies that the unitary system has a smaller equilibrium polarization P_{eq} than the non-interacting system for the same T and κ . Intuitively, this makes sense since we expect that the attractive interactions, at least for mass ratios not too much larger than 1, push the system toward an equal mixture of heavy and light particles.

Figure 10 shows the free energy per particle F/N as a function of the polarization P for $T/T_F = 10$ and three different mass ratios κ . The solid lines are cal-

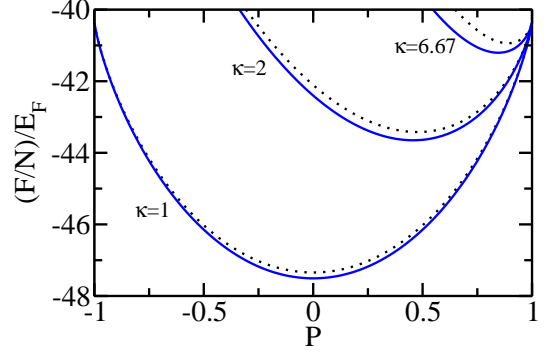


FIG. 10: (Color online) Free energy per particle F/N of the homogeneous system as a function of the polarization P for $T/T_F = 10$ and mass ratios $\kappa = 1, 2$, and 6.67 . The curves are grouped in sets of two, each labeled by their corresponding mass ratio. The solid lines are calculated using the virial equation of state at unitarity. For comparison, the dotted lines show F/N for the non-interacting system.

culated using the virial equation of state of the unitary system. For comparison, dotted lines show F/N for the non-interacting system. Since the free energy is a concave function with respect to P for fixed N and T , the equilibrium polarizations are stable minima.

To better understand the interplay of the second and third order virial coefficients for the homogeneous system, we calculate z_{eq} analogously to Eq. (32) and find P_{eq} for the homogeneous system to be

$$P_{eq} = \frac{N\lambda_{m_1}^3}{V} \left(-\text{Li}_{3/2}(-z_{eq}) \left[1 - \frac{1}{\kappa^{3/2}} \right] + [b_{2,1,\text{hom}} - b_{1,2,\text{hom}}] z_{eq}^3 \right). \quad (46)$$

Eliminating the polylogarithm function, P_{eq} can be rewritten as

$$P_{eq} = \frac{\kappa^{3/2} - 1}{\kappa^{3/2} + 1} - b_{1,1,\text{hom}} \frac{\kappa^{3/2} - 1}{\kappa^{3/2} + 1} \frac{2V}{N\lambda_{m_1}^3} z_{eq}^2 + \left[b_{1,2,\text{hom}}^{(0)} \frac{1 - 2\kappa^{3/2}}{\kappa^{3/2} + 1} + b_{2,1,\text{hom}}^{(0)} \frac{2 - \kappa^{3/2}}{\kappa^{3/2} + 1} \right] \frac{2V}{N\lambda_{m_1}^3} z_{eq}^3. \quad (47)$$

As expected, the z_{eq}^0 term depends only on the mass ratio κ and is greater than zero for $\kappa > 1$; in the limit $\kappa \rightarrow \infty$, the non-interacting system prefers to have only heavy particles, i.e., $P_{eq} \rightarrow 1$. The z_{eq}^2 term of the unitary system, in contrast, is negative for all $\kappa > 1$. This implies that the second order virial coefficient of the unitary system acts to decrease P_{eq} compared to the P_{eq} of the non-interacting system. Interestingly, the z_{eq}^3 term of the unitary system is positive for $\kappa < 5.40$ and negative

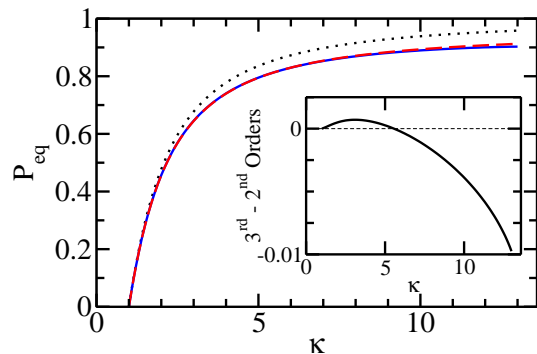


FIG. 11: (Color online) Equilibrium polarization P_{eq} of the homogeneous system at unitarity as a function of the mass ratio κ for $T/T_F = 10$. The dashed and solid lines show P_{eq} calculated using the virial equation of state up to second and third order, respectively. The dashed and solid lines are nearly indistinguishable on the scale shown. For comparison, the dotted line shows P_{eq} for the non-interacting system. The solid line in the inset shows the difference between the P_{eq} 's calculated using the virial equation of state up to the third and second orders (the dashed line shows zero as a reference).

for $\kappa > 5.40$, independent of temperature. This implies that the third order virial coefficients act to increase (decrease) P_{eq} for $1 < \kappa < 5.40$ ($\kappa > 5.40$) compared to the P_{eq} calculated using the virial equation of state up to second order.

Figure 11 shows the equilibrium polarization P_{eq} as a function of κ for $T/T_F = 10$. The dashed and solid lines show P_{eq} calculated using the virial equation of state of the unitary system up to second and third order, respectively. The second and third orders are nearly indistinguishable on the scale shown. For comparison, the dotted line shows P_{eq} for the non-interacting system. The inset of Fig. 11 shows the difference of P_{eq} calculated up to the second order subtracted from P_{eq} calculated up to the third order. Note that the zero crossing occurs at $\kappa = 5.56$, and not at $\kappa = 5.40$, since the equilibrium fugacity determined from the virial equation of state up to third order is slightly smaller than that determined from the virial equation of state up to second order.

Figure 12 shows the equilibrium polarization P_{eq} as a function of T for $\kappa = 6.67$. The dashed and solid lines show P_{eq} at unitarity calculated using the virial equation of state up to second and third order, respectively. The second and third orders are nearly indistinguishable on the scale shown. For comparison, the dotted line shows P_{eq} for the non-interacting system; it is independent of T and equals 0.89. The inset of Fig. 12 shows the difference of P_{eq} at unitarity calculated up to the second order subtracted from P_{eq} at unitarity calculated up to the third order. Since the mass ratio used is larger than 5.40, the third order correction acts to further decrease

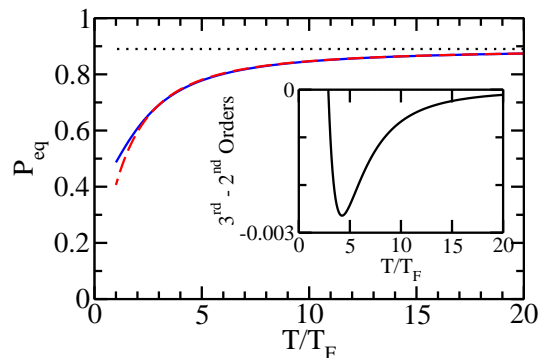


FIG. 12: (Color online) Equilibrium polarization P_{eq} of the homogeneous system at unitarity as a function of the temperature T for $\kappa = 6.67$. The dashed and solid lines show P_{eq} calculated using the virial equation of state up to second and third order, respectively. The dashed and solid lines are nearly indistinguishable on the scale shown. For comparison, the dotted line shows P_{eq} for the non-interacting system. The solid line in the inset shows the difference between the P_{eq} 's calculated using the virial equation of state up to the third and second orders.

P_{eq} for $T/T_F > 5$. Note that the virial equation of state is likely unreliable for $T/T_F \lesssim 6.67$. As the temperature decreases, interactions become more important and the deviations between P_{eq} for the unitary and the non-interacting system increase.

V. CONCLUSIONS

This paper considers the high temperature virial equation of state of unequal-mass two-component Fermi gases at unitarity. For the trapped system with equal frequencies and $\kappa > 1$, we found that the equilibrium polarization P_{eq} at unitarity is relatively small for the temperatures considered. The small deviations from $P_{eq} = 0$ are introduced by the third order virial coefficients. For the homogeneous system, in contrast, we found comparatively large P_{eq} for $\kappa > 1$. The value of P_{eq} is determined by an intricate interplay between the second and third order virial coefficients. For the cases investigated, P_{eq} increases with decreasing temperature for the trapped system while P_{eq} decreases with temperature for the homogeneous system. The fourth-order virial coefficients $b_{3,1}$ and $b_{2,2}$ for unequal-mass systems are presently unknown, preventing us to estimate the importance of higher-order terms in the virial equation of state.

At the temperatures considered, the curvature of the free energy is positive for all polarizations, thus implying the absence of any first-order phase transition. If the unequal-mass system is prepared with a polarization P different from P_{eq} , then the free energy lies above the

value it would have for P_{eq} . This suggests that the system prepared with $P \neq P_{eq}$ may phase separate when the temperature falls below a certain critical value.

In future work, it will be interesting to investigate the high temperature thermodynamics of unequal mass systems when the light and heavy species are confined by harmonic potentials with different frequencies via the local density approximation. Moreover, the treatment of cylindrically symmetric traps will be relevant for ongoing experiments. Other future extensions of our work include the treatment of unequal mass systems away from unitarity and at lower temperatures.

VI. ACKNOWLEDGEMENTS

Support by the NSF through grant PHY-0855332 is gratefully acknowledged. We also acknowledge discussions with Stefano Giorgini on the use of the local density approximation.

Appendix A: Thermodynamics of the trapped single-component fermi gas

This appendix studies the virial expansion of the single-component Fermi gas in a harmonic trap. The results for the single-component Fermi gas serve as a reference for the trapped s -wave interacting two-component Fermi gas. We first derive compact expressions for the virial coefficients, and then discuss convergence properties of the virial expansion.

Equation (7) of the main text defines the expansion coefficients b_n ; throughout this appendix, we replace n_1 by n and use a single subscript n to denote the virial coefficients b_n and the canonical partition functions Q_n . Partial derivatives of the grand canonical potential $\Omega^{(1)}$ determine the various thermodynamic quantities. The number of particles N of the single-component Fermi gas, e.g., can be expressed as a derivative with respect to the chemical potential μ ,

$$N = -\frac{\partial \Omega^{(1)}}{\partial \mu} = Q_1 \sum_{n=1}^{\infty} n b_n z^n. \quad (\text{A1})$$

To determine the coefficients b_n , we use that the population $N(E_j)$ of a state with a given single-particle energy E_j is given by the Fermi-Dirac distribution,

$$N(E_j) = \frac{1}{e^{(E_j - \mu)/(k_B T)} + 1}, \quad (\text{A2})$$

with the constraint that the total number of particles N is given by

$$N = \sum_{j=1}^{\infty} N(E_j). \quad (\text{A3})$$

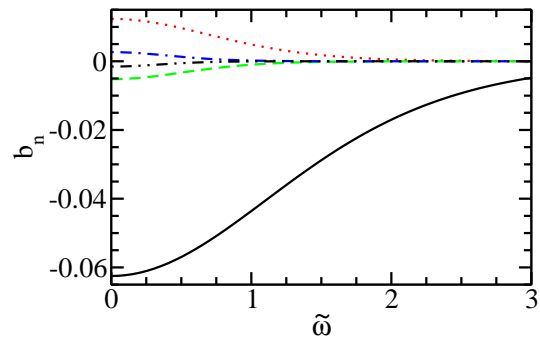


FIG. 13: (Color online) Virial coefficients b_n of the single-component harmonically trapped Fermi gas as a function of $\tilde{\omega}$. Solid, dotted, dashed, dash-dotted and dash-dot-dotted lines show b_2, b_3, b_4, b_5 and b_6 , respectively.

The single-particle energies of the three-dimensional harmonic oscillator are given by $E_j = (j + 1/2)\hbar\omega$, $j = 1, 2, 3, \dots$, and have a degeneracy of $j(j + 1)/2$. Using the single-particle energies and their degeneracies in Eqs. (A2) and (A3), we find a relationship between N , μ , and T ,

$$N = \sum_{j=1}^{\infty} \frac{j(j+1)}{2} \left[e^{(j+\frac{1}{2}-\frac{\mu}{\hbar\omega})\tilde{\omega}} + 1 \right]^{-1}. \quad (\text{A4})$$

To compare Eqs. (A4) and (A1), we Taylor expand Eq. (A4) for small z , $z = \exp[\mu/(k_B T)]$,

$$N = \sum_{j=1}^{\infty} \frac{j(j+1)}{2} \sum_{n=1}^{\infty} (-1)^{n+1} e^{-(j+\frac{1}{2})\tilde{\omega}n} z^n. \quad (\text{A5})$$

The sum over j can be done analytically. Pulling out a factor of Q_1 , we obtain

$$N = Q_1 \sum_{n=1}^{\infty} (-1)^{n+1} e^{\frac{3}{2}(n-1)\tilde{\omega}} \left(\frac{e^{\tilde{\omega}} - 1}{e^{n\tilde{\omega}} - 1} \right)^3 z^n. \quad (\text{A6})$$

Comparing Eqs. (A6) and (A1), the expansion coefficients b_n can be read off,

$$b_n = \frac{(-1)^{n+1}}{n} e^{\frac{3}{2}(n-1)\tilde{\omega}} \left(\frac{e^{\tilde{\omega}} - 1}{e^{n\tilde{\omega}} - 1} \right)^3. \quad (\text{A7})$$

Figure 13 shows the first five expansion coefficients as a function of $\tilde{\omega}$. In the low temperature limit, the b_n decay exponentially as $\exp[-3(n-1)\tilde{\omega}/2]$. The sign of b_n is given by $(-1)^{n+1}$ for all $\tilde{\omega}$ and the b_n monotonically decrease in magnitude as $\tilde{\omega}$ increases. The coefficients are even functions in $\tilde{\omega}$, i.e., b_n remains unchanged as $\tilde{\omega}$ is replaced by $-\tilde{\omega}$. Expanding Eq. (A7) for large T (small

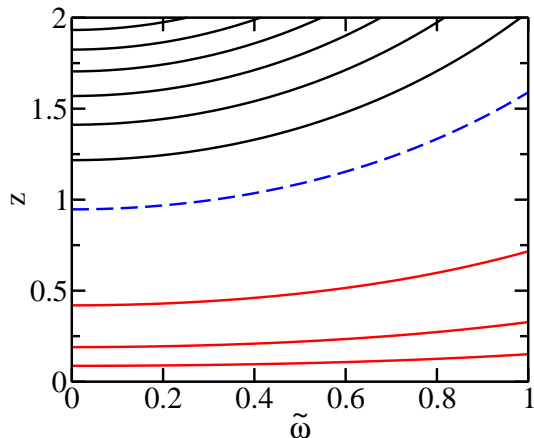


FIG. 14: (Color online) Contour plot of the percent difference $100(z + 2b_2z^2 + 3b_3z^3 - N/Q_1)/(N/Q_1)$. The dashed line shows the percent difference of 1. The solid lines below the dashed line show the percent difference in steps of powers of 10 down to a value of 0.001, while solid lines above the dashed line show the percent difference in steps of 1 up to a value of 7. We consider the region where the percent difference is less than 1 to be well converged.

$\tilde{\omega}$), we find [56]

$$b_n \approx \frac{(-1)^{n+1}}{n^4} \left[1 - \frac{1}{8}(n^2 - 1)\tilde{\omega}^2 + \frac{1}{1920}(17n^4 - 30n^2 + 13)\tilde{\omega}^4 + \mathcal{O}(\tilde{\omega}^6) \right]. \quad (\text{A8})$$

In the limit $\tilde{\omega} \rightarrow 0$ we have “universal” physics in the sense that the virial coefficients b_n approach constants, $b_n \rightarrow b_n^{(0)}$ as $\tilde{\omega} \rightarrow 0$, where $b_n^{(0)} = (-1)^{n+1}/n^4$ [39].

Figure 14 shows a contour plot of the percent difference between $z + 2b_2z^2 + 3b_3z^3$ and N/Q_1 [see Eq. (A1)]. The deviation between the exact expressions and the virial expansion is smaller than about 1% for $z \leq 1$ and is

below 5% for $z \approx 1.5$ for the range of temperatures shown. Thus, the virial expansion up to the third order provides a qualitatively correct description of the high-temperature physics for $z \lesssim 1.5$. Even though we expanded around small z , Eq. (A1) is an analytic function of z that can be continued along the positive real axis for all $z \geq 1$ [57]. For the two-component Fermi gas with pairwise interactions, in contrast, the convergence radius of the virial equation of state, to the best of our knowledge, is not known.

Lastly, one can use Eq. (A7) to calculate the Q_n for $n > 1$. A compact expression for the Q_n , $n > 1$, can be found in the literature [45, 57, 58],

$$Q_n = \sum_{\{\vec{m}\}} \prod_{i=1}^n \frac{1}{m_i!} (Q_1 b_i)^{m_i}, \quad (\text{A9})$$

where $\{\vec{m}\}$ represents all possible sets of n non-negative integers $\{m_1, \dots, m_n\}$ that fulfill the constraint

$$\sum_{i=1}^n i m_i = n. \quad (\text{A10})$$

Each set describes a unique way to divide a system of n particles into smaller clusters of m_i particles. For $n = 3$, e.g., we have the sets $\{3, 0, 0\}$, $\{1, 1, 0\}$, and $\{0, 0, 1\}$, i.e., the three-body system can be thought of as consisting of three monomers, of one monomer and one dimer, or of one trimer. For completeness, we report the expressions for the first few Q_n ,

$$Q_1 = \sum_{n=0}^{\infty} \sum_{l=0}^{\infty} (2l+1) e^{-(2n+l+3/2)\tilde{\omega}} = \frac{e^{3\tilde{\omega}/2}}{(e^{\tilde{\omega}} - 1)^3}, \quad (\text{A11})$$

$$Q_2 = b_2 Q_1 + \frac{1}{2} Q_1^2, \quad (\text{A12})$$

$$Q_3 = b_3 Q_1 + b_2 Q_1^2 + \frac{1}{6} Q_1^3, \quad (\text{A13})$$

and

$$Q_4 = b_4 Q_1 + b_3 Q_1^2 + \frac{1}{2} b_2^2 Q_1^2 + \frac{1}{2} b_2 Q_1^3 + \frac{1}{24} Q_1^4, \quad (\text{A14})$$

where we have used that $b_1 = 1$ [see Eq. (A8)].

-
- [1] P. Fulde and R. A. Ferrell, Phys. Rev. **135**, A550 (1964).
[2] A. I. Larkin and Yu. N. Ovchinnikov, Zh. Eksp. Teor. Fiz. **47**, 1136 (1964).
[3] A. I. Larkin and Yu. N. Ovchinnikov, Sov. Phys. JETP **20**, 762 (1965).
[4] S. Giorgini, L. P. Pitaevskii, and S. Stringari, Rev. Mod. Phys. **80**, 1215 (2008).
[5] C. Lobo, A. Recati, S. Giorgini, and S. Stringari, Phys. Rev. Lett. **97**, 200403 (2006).
[6] D. E. Sheehy and L. Radzihovsky, Phys. Rev. Lett. **96**, 060401 (2006).
[7] A. Bulgac and M. M. Forbes, Phys. Rev. A **75**, 031605(R) (2007).
[8] A. Recati, C. Lobo, and S. Stringari, Phys. Rev. A **78**, 023633 (2008).
[9] S. Pilati and S. Giorgini, Phys. Rev. Lett. **100**, 030401 (2008).
[10] Y. Shin, M. W. Zwierlein, C. H. Schunck, A. Schirotzek, and W. Ketterle, Phys. Rev. Lett. **97**, 030401 (2006).
[11] G. B. Partridge, W. Li, Y. A. Liao, R. G. Hulet, M. Haque, and H. T. C. Stoof, Phys. Rev. Lett. **97**, 190407 (2006).
[12] M. Iskin and C. A. R. Sá de Melo, Phys. Rev. Lett. **97**, 100404 (2006).
[13] S.-T. Wu, C.-H. Pao, and S.-K. Yip, Phys. Rev. B **74**, 224504 (2006).

- [14] C.-H. Pao, S.-T. Wu, and S.-K. Yip, Phys. Rev. A **76**, 053621 (2007).
- [15] M. M. Parish, F. M. Marchetti, A. Lamacraft, and B. D. Simons, Phys. Rev. Lett. **98**, 160402 (2007).
- [16] M. Iskin and C. J. Williams, arXiv:0810:5065v1 (2008).
- [17] A. Gezerlis, S. Gandolfi, K. E. Schmidt, and J. Carlson, Phys. Rev. Lett. **103**, 060403 (2009).
- [18] I. Bausmerth, A. Recati, and S. Stringari, Phys. Rev. A **79**, 043622 (2009).
- [19] J. von Stecher, C. H. Greene, and D. Blume, Phys. Rev. A **76**, 053613 (2007).
- [20] E. Wille, F. M. Spiegelhalter, G. Kerner, D. Naik, A. Trenkwalder, G. Hendl, F. Schreck, R. Grimm, T. G. Tiecke, J. T. M. Walraven, S. J. J. M. F. Kokkelmans, E. Tiesinga, and P. S. Julienne, Phys. Rev. Lett. **100**, 053201 (2008).
- [21] M. Taglieber, A.-C. Voigt, T. Aoki, T. W. Hänsch, and K. Dieckmann, Phys. Rev. Lett. **100**, 010401 (2008).
- [22] F. M. Spiegelhalter, A. Trenkwalder, D. Naik, G. Kerner, E. Wille, G. Hendl, F. Schreck, and R. Grimm, Phys. Rev. A **81**, 043637 (2010).
- [23] L. Costa, J. Brachmann, A.-C. Voigt, C. Hahn, M. Taglieber, T. W. Hänsch, and K. Dieckmann, Phys. Rev. Lett. **105**, 123201 (2010).
- [24] A. Ridinger, S. Chaudhuri, T. Salez, U. Eismann, D. R. Fernandes, K. Magalhães, D. Wilkowski, C. Salomon, and F. Chevy, Euro. Phys. J. D **65**, 223 (2011).
- [25] D. Naik, A. Trenkwalder, C. Kohstall, F. M. Spiegelhalter, M. Zaccanti, G. Hendl, F. Schreck, R. Grimm, T. M. Hanna, and P. S. Julienne, Euro. Phys. J. D **65**, 55 (2011).
- [26] A. Trenkwalder, C. Kohstall, M. Zaccanti, D. Naik, A. I. Sidorov, F. Schreck, and R. Grimm, Phys. Rev. Lett. **106**, 115304 (2011).
- [27] D. Blume, arXiv:1111.0941. To be published in Rep. Prog. Phys. (2011).
- [28] D. S. Petrov, Phys. Rev. A **67**, 010703(R) (2003).
- [29] F. Werner and Y. Castin, Phys. Rev. A **74**, 053604 (2006).
- [30] Y. Nishida, D. T. Son, and S. Tan, Phys. Rev. Lett. **100**, 090405 (2008).
- [31] D. Blume and K. M. Daily, Phys. Rev. Lett. **105**, 170403 (2010).
- [32] D. Blume and K. M. Daily, Phys. Rev. A **82**, 063612 (2010).
- [33] V. N. Efimov, Yad. Fiz. **12**, 1080 (1970) [Sov. J. of Nucl. Phys. **12**, 589 (1971)].
- [34] V. Efimov, JETP Lett. **16**, 34 (1972).
- [35] V. Efimov, Nucl. Phys. A **210**, 157 (1973).
- [36] E. Braaten and H.-W. Hammer, Phys. Rep. **428**, 259 (2006).
- [37] T.-L. Ho, Phys. Rev. Lett. **92**, 090402 (2004).
- [38] T.-L. Ho and E. J. Mueller, Phys. Rev. Lett. **92**, 160404 (2004).
- [39] X.-J. Liu, H. Hu, and P. D. Drummond, Phys. Rev. Lett. **102**, 160401 (2009).
- [40] H. Hu, X.-J. Liu, and P. D. Drummond, New J. Phys. **12**, 063038 (2010).
- [41] X.-J. Liu and H. Hu, Phys. Rev. A **82**, 043626 (2010).
- [42] M. Horikoshi, S. Nakajima, M. Ueda, and T. Mukaiyama, Science **327**, 442 (2010).
- [43] S. Nascimbène, N. Navon, K. J. Jiang, F. Chevy, and C. Salomon, Nature **463**, 1057 (2010).
- [44] D. A. McQuarrie, Statistical Mechanics, University Science Books, California, 2000.
- [45] K. Huang, *Statistical Mechanics, 2nd Ed.* (John Wiley and Sons, Inc., New York, 1963).
- [46] Our notation differs from that employed in Refs. [39] and [41]. The second and third order virial coefficients for the trapped equal-mass system are denoted by Δb_2 and Δb_3 in Ref. [39]. The relationship between our b_{n_1, n_2} and the Δb_n of Ref. [39] for equal masses is $\Delta b_2 = b_{1,1}/2$ and $\Delta b_3 = (b_{1,2} + b_{2,1})/2$. Moreover, our $Q_{1,0}$ is by a factor of 2 smaller than the Q_1 reported in [39].
- [47] For the harmonically trapped gas, where atoms of species 1 and 2 feel the same trapping frequency, one finds $Q_{1,0} = Q_{0,1}$ (and more generally, $Q_{n_1,0} = Q_{0,n_2}$ for $n_1 = n_2$) and Eqs. (10)-(12) can be simplified. For the homogeneous system, in contrast, $Q_{1,0}$ and $Q_{0,1}$ differ if $m_1 \neq m_2$. Our definition of the virial coefficients is chosen such that it applies to the trapped and homogeneous systems.
- [48] T. Busch, B.-G. Englert, K. Rzazewski, and M. Wilkens, Found. Phys. **28**, 549 (1998).
- [49] F. Werner and Y. Castin, Phys. Rev. Lett. **97**, 150401 (2006).
- [50] O. I. Kartavtsev and A. V. Malykh, J. Phys. B **40**, 1429 (2007).
- [51] S. T. Rittenhouse, N. P. Mehta, and C. H. Greene, Phys. Rev. A **82**, 022706 (2010).
- [52] X. Leyronas, Phys. Rev. A **84**, 053633 (2011).
- [53] See supplementary material at [XXX].
- [54] As can be seen from the expression for T_F , the Fermi temperature of the trapped non-interacting system is independent of the mass of the constituents and our reference Fermi temperature can alternatively be interpreted as the Fermi temperature of the single-component Fermi gas with $N/2$ particles of mass m_2 . For the homogeneous system (see Sec. IV), in contrast, the Fermi temperature depends on the mass of the constituents and we define T_F in terms of m_1 in that case.
- [55] C. Menotti, P. Pedri, and S. Stringari, Phys. Rev. Lett. **89**, 250402 (2002).
- [56] Ref. [39] does not include the term proportional to $\tilde{\omega}^2/n^4$.
- [57] B. Kahn and G. E. Uhlenbeck, Physica **5**, 399 (1938).
- [58] J. E. Mayer and M. G. Mayer, *Statistical Mechanics 3rd Ed.* (John Wiley and Sons, Inc., New York, 1940), Chapter 13.

Auxiliary material for “Thermodynamics of the trapped two-component Fermi gas with unequal masses at unitarity”

K. M. Daily¹ and D. Blume¹

¹*Department of Physics and Astronomy, Washington State University, Pullman, Washington 99164-2814, USA*

(Dated: October 26, 2018)

This material tabulates the expansion coefficients $b_{1,2}^{(n)}$ and $b_{2,1}^{(n)}$ ($n = 0, 2, 4,$ and 6) of the two-component unequal-mass Fermi gas in a harmonic trapping potential at unitarity. The calculation of the virial coefficients $b_{1,2}$ and $b_{2,1}$ requires the eigenvalues $s_{l,\nu}$ [see Eqs. (21)-(24) of the main text]. We calculate the first 10,000 $s_{l,\nu}$ for each l , $l = 0 - 50$, and each mass ratio considered. To obtain the accuracy reported in Tables I and II, we must maintain a higher working precision than machine precision. We use Mathematica to determine the $s_{l,\nu}$ with an accuracy of about one part in 10^{80} (most likely, a notably reduced precision would work just as well). To obtain the $b_{1,2}^{(n)}$ and $b_{2,1}^{(n)}$, we Taylor expand Eqs. (23) and (24) of the main text to high order at a finite but small $\tilde{\omega}$. The $\tilde{\omega}$ is chosen such that $b_{1,2}$ and $b_{2,1}$ are converged at that value; note, since we use a cutoff in ν and l , we cannot Taylor expand around $\tilde{\omega} = 0$. To determine the expansion coefficients for $\tilde{\omega} = 0$, we rewrite the Taylor expanded series in the form of Eq. (25) of the main text. For all values listed in Tables I and II, the error is indicated by the value in parentheses.

arXiv:1110.1400v2 [cond-mat.quant-gas] 12 Mar 2012

TABLE I: High temperature expansion coefficients $b_{1,2}^{(0)}$, $b_{1,2}^{(2)}$, $b_{1,2}^{(4)}$, and $b_{1,2}^{(6)}$ for one heavy fermion and two light fermions for various mass ratios κ . The odd order coefficients are zero to the calculated accuracy. For the mass ratio of 13.607, we use 67907169/49906069.

κ	$b_{1,2}^{(0)}$	$b_{1,2}^{(2)}$	$b_{1,2}^{(4)}$	$b_{1,2}^{(6)}$
∞	-1/8	3/32	-3/64	157/7680
≈ 13.607	-0.1148983967419143(1)	0.0822846200355016(1)	-0.0387505068487700(1)	0.0157412555073196(1)
12	-0.1137494461215969(1)	0.0810220572507766(1)	-0.0378883247633289(1)	0.0152623106544741(1)
10	-0.1118930949742869(1)	0.0790006163965818(1)	-0.0365219657732420(1)	0.0145117031903192(1)
8	-0.1092998807903862(1)	0.0762155583916566(1)	-0.0346683837395572(1)	0.0135104326391047(1)
6.67	-0.1069167194627094(1)	0.0736967168785517(1)	-0.0330216423362948(1)	0.0126379464141623(1)
6	-0.1054166227589069(1)	0.0721315542690726(1)	-0.0320129640005759(1)	0.0121117516797285(1)
4	-0.0989274431349124(1)	0.0655479723141608(1)	-0.0278982228513893(1)	0.0100342277821471(1)
2	-0.0854120042021242(1)	0.0528794100025025(1)	-0.0206256339544718(1)	0.0066746031546180(1)
1	-0.0683396093112849(1)	0.0388697595336693(1)	-0.0136736950010533(1)	0.0039221710096865(1)

TABLE II: High temperature expansion coefficients $b_{2,1}^{(0)}$, $b_{2,1}^{(2)}$, $b_{2,1}^{(4)}$, and $b_{2,1}^{(6)}$ for two heavy fermions and one light fermion for various mass ratios κ . The odd order coefficients are zero to the calculated accuracy. For the mass ratio of 13.607, we use 67907169/49906069.

κ	$b_{2,1}^{(0)}$	$b_{2,1}^{(2)}$	$b_{2,1}^{(4)}$	$b_{2,1}^{(6)}$
1	-0.0683396093112849(1)	0.0388697595336693(1)	-0.0136736950010533(1)	0.0039221710096865(1)
2	-0.0392970167749193(1)	0.0168593086798205(1)	-0.0035955339421578(1)	0.0002304139076276(1)
3	-0.0043665570747450(1)	-0.0113457745372200(1)	0.010983366385180(9)	-0.0062006157599(2)
4	0.039557237585138(3)	-0.0500118892685(1)	0.034191104164(3)	-0.01875475605(4)
5	0.09356648286595(9)	-0.101149373357(4)	0.0692162284(1)	-0.041313819(2)
6	0.158595249651(2)	-0.16632882903(7)	0.119273264(2)	-0.07878135(4)
6.67	0.208903183724(6)	-0.2185938559(4)	0.162900512(9)	-0.1152027(2)
7	0.23583203496(2)	-0.2470369251(7)	0.18775226(2)	-0.1372414(4)
8	0.32697976919(7)	-0.344820636(4)	0.2782550(2)	-0.224063(3)
9	0.4346241735(3)	-0.46141279(2)	0.3946117(6)	-0.34799(2)
10	0.562958249(2)	-0.59892409(7)	0.540902(3)	-0.51922(5)
11	0.719509561(4)	-0.7602484(2)	0.721507(7)	-0.7495(2)
11.5	0.812728781(5)	-0.8511988(4)	0.82616(2)	-0.8909(3)
12	0.920430123(8)	-0.9502037(6)	0.94125(2)	-1.0522(5)
12.25	0.98168666(1)	-1.0031950(7)	1.00295(3)	-1.1410(6)
12.5	1.04968722(2)	-1.0589100(9)	1.06756(4)	-1.2350(8)
12.75	1.12681250(2)	-1.117846(2)	1.13521(4)	-1.336(1)
13	1.21738420(2)	-1.180858(2)	1.20609(5)	-1.443(2)
13.1	1.25917000(2)	-1.207546(2)	1.23540(6)	-1.487(2)
13.2	1.30557689(3)	-1.235350(2)	1.26530(6)	-1.533(2)
13.3	1.35844252(3)	-1.264602(2)	1.29590(7)	-1.579(2)
13.4	1.42130482(3)	-1.295930(2)	1.32710(7)	-1.627(2)
13.5	1.50304784(3)	-1.330880(2)	1.35930(8)	-1.676(2)
13.51	1.51310826(3)	-1.334720(2)	1.36250(8)	-1.681(2)
13.52	1.52371358(3)	-1.338657(2)	1.36580(8)	-1.686(2)
13.53	1.53496097(3)	-1.342707(2)	1.36920(8)	-1.691(2)
13.54	1.54698040(3)	-1.346893(2)	1.37250(8)	-1.696(2)
13.55	1.55995276(3)	-1.351246(2)	1.37590(8)	-1.701(2)
13.56	1.57414297(3)	-1.355809(3)	1.37930(8)	-1.706(2)
13.57	1.58996766(3)	-1.360653(3)	1.38270(8)	-1.711(3)
13.58	1.60815453(3)	-1.365900(3)	1.38620(8)	-1.716(3)
13.59	1.63021654(3)	-1.371803(3)	1.38970(8)	-1.721(3)
13.595	1.64379580(3)	-1.375185(3)	1.39160(8)	-1.724(3)
13.596	1.64683813(3)	-1.375916(3)	1.39190(8)	-1.724(3)
13.597	1.65002366(3)	-1.376671(3)	1.39230(8)	-1.725(3)
13.598	1.65337456(3)	-1.377454(3)	1.39270(8)	-1.725(3)
13.599	1.65691940(3)	-1.378269(3)	1.39310(8)	-1.726(3)
13.6	1.66069607(3)	-1.379124(3)	1.39350(8)	-1.726(3)
13.601	1.66475668(3)	-1.380025(3)	1.39390(8)	-1.727(3)
13.602	1.66917640(3)	-1.380987(3)	1.39430(8)	-1.727(3)
13.603	1.67407090(3)	-1.382028(3)	1.39470(8)	-1.728(3)
13.604	1.67963563(3)	-1.383182(3)	1.39510(8)	-1.728(3)
13.605	1.68625428(3)	-1.384511(3)	1.39550(8)	-1.729(3)
13.606	1.69493193(3)	-1.386183(3)	1.39600(8)	-1.729(3)
≈ 13.607	1.71529815(3)	-1.389797(3)	1.39670(8)	-1.730(3)